

Crypts detection in microscopic images using hierarchical structures

Cristian Smochina¹, Vasile Manta¹
and Walter Kropatsch²

¹ Faculty of Automatic Control and Computer Engineering,
"Gheorghe Asachi" Technical University of Iasi, Romania
smochina.cristian@yahoo.com, vmanta@cs.tuiasi.ro

² Pattern Recognition and Image Processing Group, Institute of Computer Graphics and Algorithms,
Vienna University of Technology, Austria
krw@prip.tuwien.ac.at

Abstract. This paper presents an extended and improved version of an automatic technique which robustly identifies the epithelial nuclei (crypt) against interstitial nuclei in microscopic images taken from colon tissues. The detection of the crypt inner boundary is performed using the closing morphological hierarchy. The disadvantages of this approach related to the execution time and the used memory are highlighted and the morphological pyramid is used instead due to its computational efficiency, the reduced amount of used memory and the increased robustness. An analysis of the two approaches is performed considering the number of processed pixels, the used memory and the complexity. The outer border is determined by the epithelial nuclei overlapped by the maximal isoline of the inner boundary. The percentage of the mis-segmented nuclei against epithelial nuclei per crypt is used to evaluate the proposed methods. The limitations are described in order to highlight the situations in which the current approaches do not provide suitable results.

Keywords: Crypt segmentation, Morphological hierarchy, Morphological Pyramid, Biomedical imaging, Pathology, Microscopy.

1 Introduction

The image processing techniques are successfully applied in biomedical research because they allow large scale statistical evaluation in addition to classical eye screening evaluation. The complex diagnostic process can be enhanced by providing the pathologists with quantitative data extracted from images. This is needed because a diagnostic is given after a large set of biological samples are analysed (tissues stained with different markers).

The microscopic image segmentation can be used in both sections of the pathology: cytology (the study of cells) and histology (anatomical study of the microscopic structure of tissues) [2]. This segmentation is difficult due to the low contrast and weak boundaries on out-of-focus nuclei, different grey values for the background, non-uniform distribution of material inside the nucleus caused, considerable variation of object features (shape, size, orientation) and different nuclei distribution within the epithelial layer [3].

This paper is organized as follows. This section points out the goal of this study. The inner boundaries of the crypts are detected using the morphological hierarchy (section 2) [1]. The method drawbacks and the motivation for a different approach are presented in sub-section 2.4. In section 3 the same task is more efficiently accomplished using the morphological pyramid. Sub-section 3.4 presents a comparison between these two structures. The outer borders and the lumen validation are performed in section 4. The results are evaluated in section 5 and concluded in Section 6. The sub-section 5.1 provides addition discussions regarding the limitations of the proposed methods and the conditions that the images must fulfil to obtain proper results.

1.1 State of the art

The difficulty in segmenting the microscopic images is related to the approach used to solve the mentioned problems. The introduced techniques from the literature cover fields like microscopy, biomedical engineering and imaging, bioinformatics or pattern recognition [3]. Since the studies are related with the cytology and histology, many studies address the nuclei segmentation ([2], [3]) but also the segmentation of histological structures like gland or crypt similar to this paper.

In [4] a threshold is used to identify the gland seeds which are grown to obtain the nuclei chain. In [5] the pixel labelling to different classes is performed using a clustering approach based on the textural properties. An

object-graphs approach is described in [6] where the relationship between the primitive objects (nucleus and lumen) is considered. The prostate cancer malignancy is automatically graded (Gleason system) in [7] after the prostate glands are detected.

In the proposed techniques from this study, the hierarchical representation of the image plays an important role and has been often used in medical image processing. In [14] the mammographic images are hierarchically decomposed into different resolutions and segmented by analysing the coarser resolutions. Also the multi-resolution wavelet analysis [15] and the Gaussian multi-resolution segmentation technique [16] are used.

1.2 Aim of the study

In pathology the areas covered by epithelial nuclei from a tissue section provide important clinical clues about the health and the disease evolution for a patient. The epithelial layer (with epithelial nuclei) is part of the crypt (Fig. 1a) and surrounds the lumen which is an empty area [8]. The stroma areas are placed between crypts (Fig. 1a) and contain isolated cells with non-regular shape and without particular patterns of arrangement.

The crypts from fluorescence images of colorectal tissue sections are segmented with the proposed specific techniques. We used 8 bit greyscale images (Fig. 1a) containing nuclei labelled with DAPI, a fluorescent stain that binds strongly to DNA [9] and acquired using a TissueFAXS slide scanner (TissueGnostics, Austria).

Our objective is to directly find the boundaries of the crypts (i.e. the epithelial layer), without dealing with the epithelial nuclei (Fig. 2). One alternative approach is to segment each nucleus and to analyse the structures that they form but this approach can encounter additional problems.

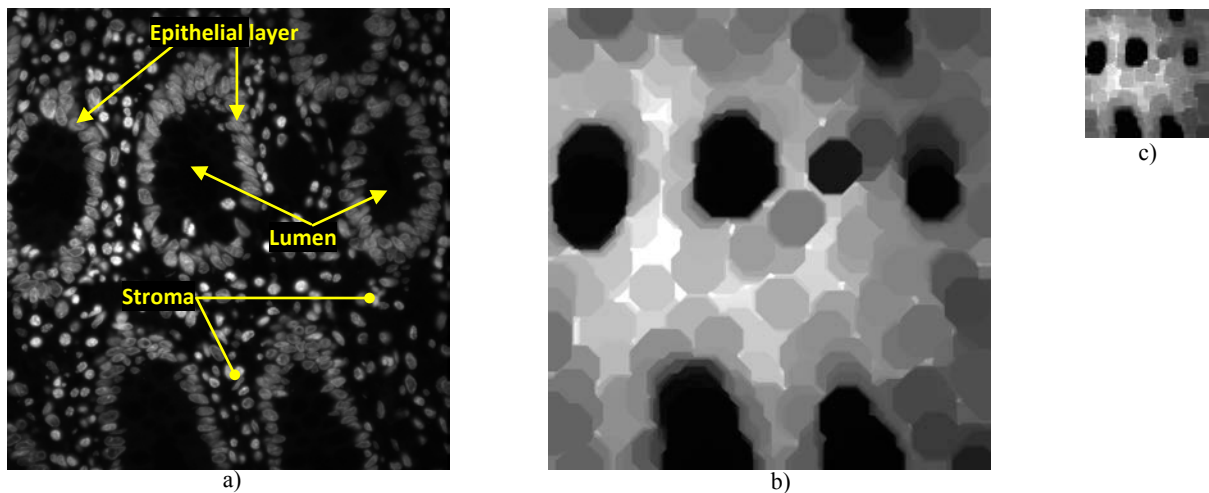


Fig. 1. a) Fluorescence image with crypts from a colon tissue section. b) The image from the top level of the morphological hierarchy; the black regions indicate the lumen. c) The image from the critical level (5th level) of the morphological pyramid, enlarged for better visualization.

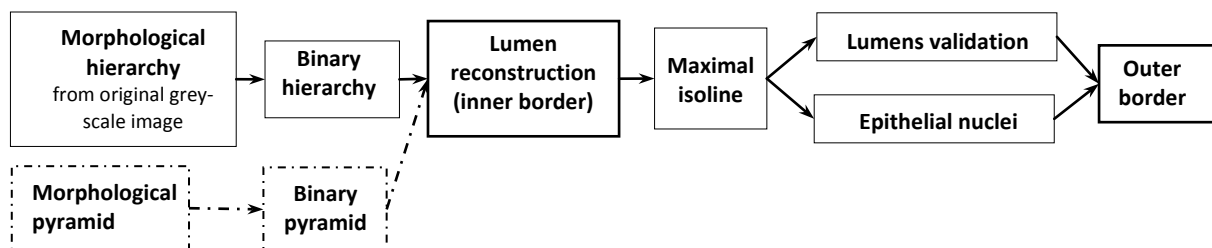


Fig. 2. Overview scheme of the proposed techniques using the morphological hierarchy and the pyramid (dashed).

2 Lumens segmentation using the morphological hierarchy

The biological information is very important in designing the segmentation technique. Without considering the arrangements of the objects of interest (in this case the crypts) in their natural environment (tissue), it would not be possible to select the right approach and the proper filters over the image. The high level information (e.g. the ring like shape of the crypt) is considered together with the nuclei distribution over different region

types. The lumen does not contain nuclei and appears like a big round black area surrounded by a ‘ring’ with variable thickness. This ring contains a high density of touched/chained epithelial cells. The exceptional cases appear when the lumen gets to be in touch with the stroma area due to missing cells that ‘break’ this ring.

In order to fill these gaps/‘breaks’ (do not exceed the size of 1-2 nuclei) the nuclei from the crypts must be connected. By applying the morphological closing operation (section 2.1) on the grey image, the nuclei closer than the size of the used kernel will be connected. Since the breaks have different sizes, this filtering operation is applied multiple times with different kernel sizes. This leads as to the hierarchical image representation (section 2.2, without the sub-sampling step [12]) where each level is obtained by applying the closing operation with an increasing size on the base image. This ensures that all gaps sizes are filled.

This hierarchical decomposition allows easy access to *global* but also to *local* information (pixel grey values or gradient). In order to ignore the unnecessary details and to keep only the important information, the relations between the crypt components (epithelial layer and lumen), the stroma and the background are considered. The *global* information like the region’s size and relation with the other region types is utilised because the low level cues will not be able to separate the regions having a particular meaning [10].

2.1 Morphological closing operator

The morphological closing operation [11] (let \bullet denote this operation) fuses narrow breaks, smooths the objects’ boundary, eliminates small holes, fills gaps in the contour and removes the dark holes smaller than the structure element (SE). The geometrical interpretation of the operation can be used for a better understanding. If the SE is considered a disk (“rolling ball” with radius r , Fig. 3a), the boundary is established by the points from SE’s border (disk’s border) closest to the border of the object as SE is rolled on the outside of the object.

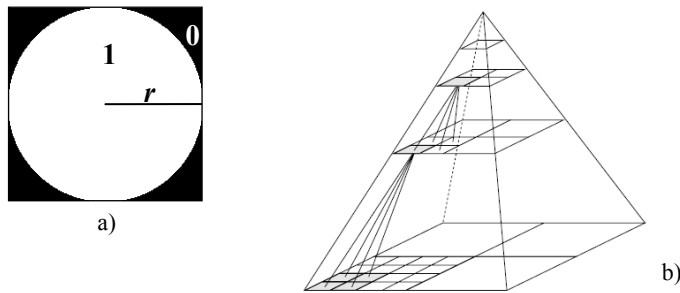


Fig. 3. a) The SE as a disk with the radius r .
b) A $2 \times 2 / 4$ regular pyramid [10].

This geometrical fitting property of the closing operation takes us to the *r-regular* partition [19]. By considering the general round shape of a lumen, we can relate the maximum size of the gap (2 nuclei) with a disk of radius equal to the size of a nucleus. In a non-rigorous explanation, the limitation of the method can be formulated Γ_1 : if a disk of a radius bigger than the size of a nucleus can be ‘rotated’ within this break, then the method is not applied (because this situation is not according to the considered biological limitation).

According to [19] a binary region is called *r-regular* when at every boundary point exist two osculating disks of radius r which are entirely in the foreground and background respectively. Basically, the regions could be morphologically open and closed using disks of radius smaller than r such that the curvature doesn’t exceed $1/r$. This rule is proper to be used in our case if we consider the nuclei area as being the foreground. Still, the rolling disk should be only on the background (to include the epithelial layer breaks) because no assumption can be precisely made about the epithelial layer (this can have various thickness, e.g. Fig. 1a). The *r-halfregular* regions which are less restricted: the osculating r -disks could exist only in the foreground or only in the background, and the number of regions (connected components) must not change by morphologically opening or closing with disks of radius smaller than r . In our case we consider that the *r-disk* is osculating within the background, i.e., within breaks. If we relate the *r-disk* to the previous rule, r should be the diameter of a nucleus. More than that, this region should be a maximal *r-halfregular*, i.e., there is no other $r' > r$ such that the region is *r'-halfregular*. This rule says that the method is not applicable for *r'-halfregular* regions with $r' > r$.

2.2 Morphological hierarchy

The hierarchical representation is built using the closing operation applied by increasing the size of the SE according to the level of the hierarchy. In the lower levels only the small gaps will be filled while the bigger ones will be closed in the upper levels.

Let consider the SE ψ_r as a two-dimensional disk of diameter $2r+1$ (r is the radius of the disk, Fig. 3a). If I denotes the input grey scale image, each level $\ell > 0$ of the hierarchical morphological representation H_\bullet (with of L_\bullet levels) is given by $H_\bullet^\ell = H_\bullet^1 \bullet \psi_{2^\ell}, \ell = \overline{1, L_\bullet}$; $H_\bullet^1 = I$.

The lumens should ‘survive’ till the top level (Fig. 1b) and should be easier highlighted; also the gaps from the crypts should be filled. The maximum number of levels L_\bullet is established by limiting the SE’s size so that it covers maximally 2-3 nuclei. Approximating the diameter of a nucleus with 30 pixels, the maximum SE that must be used is established to a disk of diameter 101 (ψ_{50}) which gives 25 levels.

2.3 Binary hierarchy and lumen reconstruction

In the morphological hierarchy the lumen positions can be easier detected in the higher levels but the lower levels give more details. The proper reconstruction of each lumen is done by analysing the lower levels of the hierarchy where more details are present but using the found regions from the top level.

Since in the top level the lumens can be easily detected by a simple thresholding, a binary hierarchy H_{bw} (also with L_\bullet levels) is built in which each level represents the result of thresholding applied on the corresponding level from the H_\bullet . Each level l is given by $H_{bw}^l = H_\bullet^l < c \cdot thr_{Otsu}(H_\bullet^l), l = \overline{1, L_\bullet}$ where $thr_{Otsu}(\cdot)$ computes the threshold using the Otsu’s method [13] and $0 < c \leq 1$ (0.5 in our experiments).

In H_{bw} , a vertical relation between partitions of successive levels can be established: each partition of a level is included in a partition from the below level. According to this rule, for each partition of the top level, the corresponding lower level can be found such that the descendent partition from this level properly identifies the lumen [1].

The border of the found lumens actually describes the inner border of the crypt (Fig. 4a). The false positive (FP) results are eliminated by a validation rule in section 4.

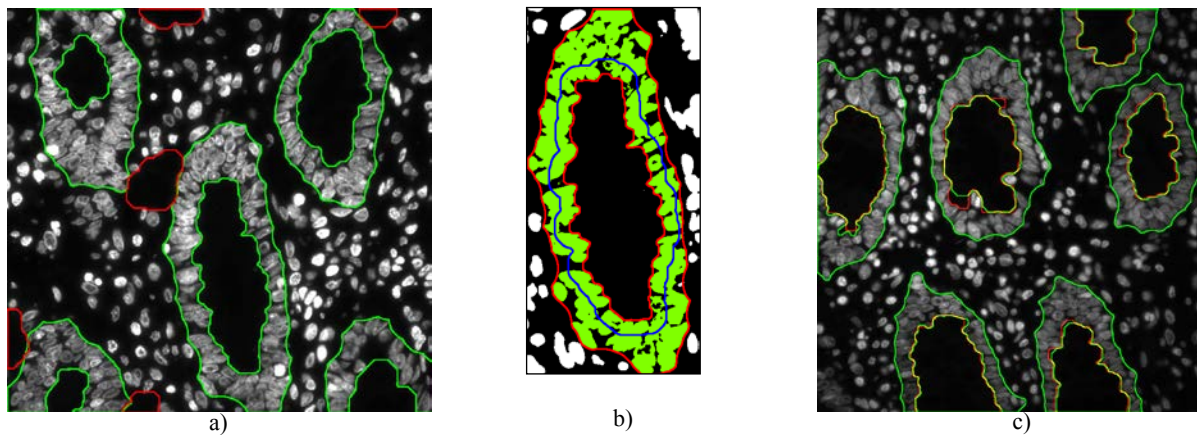


Fig. 4. a) The true positive (green curves) and the false positive (red curves) lumen boundaries. b) The boundaries (red curves) of the crypt from the middle of Fig. 1a and its maximal isoline (blue curve) which gives the maximum sum of the pixels intensities. c) The interior boundaries obtained using the morphological hierarchy (green curves) and the pyramid (red curves); the results are identical on the yellow portions. The outer borders are depicted with green.

2.4 Drawbacks

The morphologic closing operator was applied on the original image to obtain each level of the hierarchy (section 2.2). Since the closing is an idempotent operation (its reapplication produces no further changes to the previously result) [12], the size of the SE grows according to the hierarchy levels so that the bigger gaps to be filled in the higher levels while the image size remains constant.

This technique provides stable results [1] but presents some solvable problems ($p1$, $p2$ and $p3$) [17]. It makes use of a high number of levels (25); each level is actually an image with the same size as the original one. The used memory linearly increases (section 3.4) by adding levels to the hierarchy ($p1$). The closing operator applied with increasing SE increases the computation time (section 3.4) for each level as moving to the top of the hierarchy ($p2$).

These problems motivated a search for another approach to deal more easily with the big amount of data, to reduce the computation time and the used memory but in the same time to preserve or even enhance the quality of the results. A constant SE can be used on the sub-sampled image to reduce the computation time. A representation structure in which the image size is reduced is the pyramid. The pyramid of an image describes its content at multiple levels of resolution [10].

3 Lumens segmentation using the morphological pyramid

The multi-resolution representation has been used with success in image processing and proved their computational efficiency in data representations and processing ([14], [15], [16]). This stack of images with exponentially decreasing resolutions allows easy access to different resolutions of an image making this a good reason to be used in processing high amount of data [17].

An image pyramid (Fig. 3b) describes the content of an image at multiple levels of resolution [12] having the input image at the base level. Successive levels reduce the size of the data by a reduction factor $\lambda > 1$. The reduction window relates one pixel from a level with a set of pixels in the level directly below. The content of a lower resolution pixel is computed using the reduction function having as input the pixels within the reduction window. Two successive levels of a pyramid are related by the reduction window and the reduction factor. Based on this relation, for each pixel of the pyramid from any level the receptive field (RF) can be computed.

The $RF(l)$ aggregates all pixels in the base level for which p_i^l (pixel i from level l) is the ancestor.

The regular pyramids are characterized by constant reduction window and constant reduction factor. In this case the number of levels is limited by the reduction factor: $L_{\max} = \log(\text{image_size})/\log(\lambda)$. The usually notation $n \times n / \lambda$ for a regular pyramid indicates a reduction factor of λ and as reduction window a square $n \times n$, i.e. $n \times n$ pixels are associated to a single pixel from the level directly above. The main computation advantage of regular pyramid is due to their logarithmic complexity; a more detailed analysis and justification of using the sampled domain instead of un-sampled domain is presented in section 3.4.

3.1 Maximum levels of the pyramid

Due to the advantages of the morphological closing (section 2.1), the pyramid is built using this operator. In this case, the receptive field of a pixel p_l from level l is determined based on the used SE. If the SE for the closing operator is a disk of diameter $2r + 1$ (r is the radius of the disk), we determined the following formula to compute the RF for a pixel from level l :

$$|RF(l)| = 2^{l-1} \cdot (\pi \cdot r^2) + |RF(l-1)| - 2^{l-2}; l > 2 \quad (1)$$

where $|\cdot|$ computes the area of a region. The receptive field for the pixels from level 2 is given by the SE's area:

$|RF(p_2)| = \pi \cdot r^2$ and $|RF(p_1)| = 1$. For example, considering ψ_3 as SE, the RF of a pixel from the second level has the size 28 pixels (the area of a disk with radius 3), $|RF(p_3)| = 138$ respectively $|RF(p_4)| = 358$.

The RF for any pixel of the pyramid grows as the reduction window increases. The computation of the pixel's RF from the higher levels of the pyramid could be considered a top-down process by computing the equivalent closing kernel. Reversing this process, having an object of a certain size, based on (1) we could estimate the level of the pyramid in which this object will 'disappear', i.e., to be merged with other objects/background.

For instance, if in the base image there is a round object with the area of 300 pixels, according to the previous concrete example, this will be visible in the third level ($|RF(p_3)| < 300$) but will 'disappear' in the fourth level ($300 < |RF(p_4)|$). For this example, in the third level there is a pixel which corresponds only to this object. In the fourth level the receptive field of any pixel is bigger than the object; this means that any receptive field includes the object but also other information or portions from other objects or background.

Suppose that the input image contains n_o objects to be detected and $l_{o_i}, i = \overline{1, n_o}$ represents the level after which the object o_i will 'disappear' (i.e., $|RF(l_{o_i})| \leq |o_i|$ and $|o_i| < |RF(l_{o_i} + 1)|$). Based on this information, the maximum number of pyramid levels to be computed is given by

$$L_{\Pi} = \max \{l_{o_i}; i = \overline{1, n_o}\} \quad (2)$$

This represents the minimum number of levels which gives all the necessary information to perform the segmentation and reduces the used memory ($L_{\Pi} < L_{\max}$) and the computation time (Γ_2).

3.2 Morphological pyramid

One level of the morphological pyramid is obtained in two steps: firstly the current level is morphologically filtered with the SE $\psi_{r_{\Pi}}$, secondly the result is sub-sampled to obtain the next level. The morphological pyramid Π consists of L_{Π} levels and each level $\ell > 0$ is given by:

$$\Pi^{\ell} = (\Pi^{\ell-1} \bullet \psi_{r_{\Pi}}) \downarrow_4, \ell = \overline{2, L_{\Pi}}, \Pi^1 = I \quad (3)$$

The \downarrow_4 denotes the sub-sampling process which reduces the image size by four, i.e. $\lambda = 4$.

The question is, if by making use of this computation efficiency the quality of the results would be the same or even similar with the results reported in [1]. Similar to the morphological hierarchy where the maximum level ($L_{\bullet} = 25$) gives the proper partitions from which the lumens are reconstructed, in case of the pyramid a suitable resolution level must be selected. From experimental tests resulted that the 5th level (critical level) is the maximum level of the pyramid which offers the minimum details to extract relevant information.

In order to relate the closing operation in the sampled (pyramid Π) and the un-sampled (hierarchy H) domain, the level H^{25} of the hierarchy must be related with the level Π^5 of the pyramid; this implies the relation between the SEs ψ_{50} and $\psi_{r_{\Pi}}$ [17]. Since the SE ψ_{50} was chosen to cover maximally 2-3 nuclei, the same rule must be also applied for the 5th level of the pyramid. The relation between the level l_H of the hierarchy and the level $l+1$ of the pyramid is given by:

$$(H^{l+1} \bullet \psi_{l_H}) \downarrow_{4^l} \approx (\Pi^{l+1} \bullet \psi_{\frac{l_H}{2^{l-1}}}) \downarrow_4 \quad (4)$$

The previous equation indicates that the SE ψ_7 must be used leading to a $15 \times 15/4$ regular pyramid.

Similar to section 2.3, a binary pyramid Π_{bw} is built in which each level represents the result of the thresholding applied on the corresponding level from Π . For the pyramid, the descendent partitions of the Π_{bw}^5 from the level Π_{bw}^3 properly identifies the lumens. The false positive results are eliminated in section 4.

3.3 Critical levels

To rule Γ_2 (section 3.1) plays an important role in selecting the critical level. The 5th level has been experimentally chosen because it provides the best results. Using Γ_2 , the critical level can be predicted based on the object sizes and the used SE (equation (2)).

The major impact of this rule is that the robustness of the method can be improved. In the binary pyramid the level Π_{bw}^3 has been chosen because it properly identifies all lumens. Using the information provided by Γ_2 , for each object size a certain level can be choose increasing the detection accuracy; a concrete example is described in section 5.1. Also the method limitations can be mathematically formulated by restricting the objects to be detected on a certain level based on their RF's size:

$$\left\{ \begin{array}{ll} RF_{size} < s_{\min}^l, & \text{no detection} \\ s_{\min}^l \leq RF_{size} < s_{\max}^l, & \text{object detected} \\ RF_{size} \geq s_{\max}^l, & \text{disappearance} \end{array} \right. \quad (5)$$

According to (5), at level l only the objects having the RF in the range $\left[s_{\min}^l, s_{\min}^l\right)$ will be detected. If the RF is above this limit, the object ‘disappeared’ i.e. merged with other objects/background. This provides the application limitations of this approach on images with different sizes for the objects.

3.4 Moving from un-sampled to sampled domain

Fig. 5a shows the difference between the numbers of accessed pixels (NAP) for building the two morphological structures. The NAP decreases exponentially as going to the top levels in the pyramid’s case, while for the hierarchy the NAP increases based on a quadratic polynomial [17].

Regarding the time complexity, the same graphic can be used because the execution time is related to the number of accessed pixels. A time execution graphic would keep the same shape but the ordinate will indicate the execution times. For both structures, the complexity for creating a level is the same $O(p^2 \cdot n^2)$, i.e. the computational complexity of the morphological closing, where p is the maximum between the width and height of the image and n is the diameter of the used SE. In case of the hierarchy, n increases, while in case of pyramid p decreases as going to the higher levels.

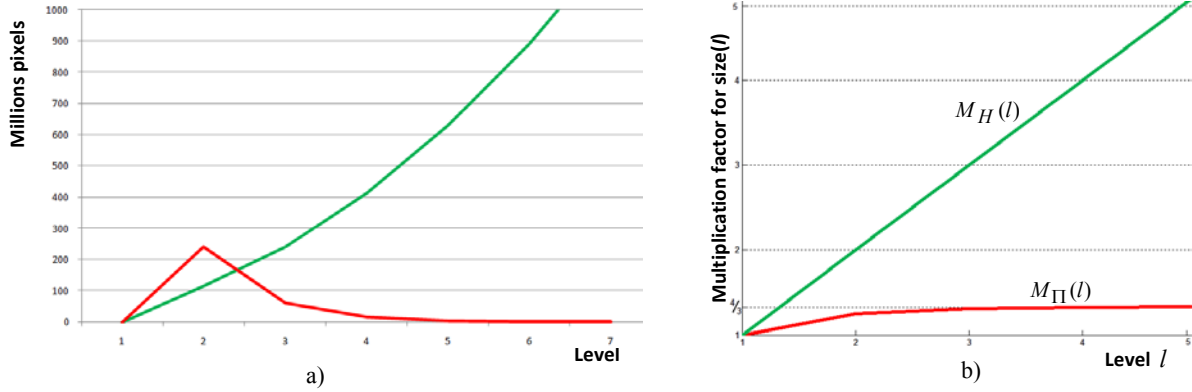


Fig. 5 a) The number of pixels accessed per level to compute the morphological pyramid (red) and the morphological hierarchy (green). b) The memory used (in terms of $size(I)$) to create the morphological pyramid (red) and the morphological hierarchy (green).

For the un-sampled hierarchical representation, each level has the same size of the first level, i.e. the size of the input image $size(I)$. This means that the used memory increases linear by adding level to the hierarchy. The total memory used to create the hierarchy is $M_H(L_\bullet) = L_\bullet \cdot size(I)$.

In case of using the pyramid, the amount of used memory has been considerably reduced. A new level is obtained by reducing the image from the level immediately below by a factor λ . The total used memory to represent a level l is $M_\Pi(l) = \left(1 + \frac{1}{2^2} + \frac{1}{2^4} + \dots + \frac{1}{2^{2 \cdot l}}\right) \cdot size(I)$. In [20] it was proved that $M_\Pi(l) < \frac{4}{3}|I|, \forall l$.

Fig. 5b shows how the used memory increases when building both hierarchical structures. The ordinate indicates how the used memory increases (in terms of the original image’s size) as adding levels to the structure. For instance, considering the size of the images used in our experiments $size(I) = 0.9$ MB, the first 5 levels of the hierarchy needs $5 \cdot size(I) = 4.5$ MB while the pyramid needs less than $1.33 \cdot size(I) = 1.2$ MB.

4 Crypt’s outer border

The FP lumens appear due to large black areas within the stroma. They are eliminated by observing the high nuclei density around the lumens: the crypt’s nuclei are packed tightly together while those from the stroma areas are wide spread with considerable distances between them. The isolines of the inner boundary are used to eliminate the FP lumens and to detect the outer border which delineates the epithelial nuclei [1].

The lumen validation is performed by intersecting the maximal isoline with the area covered by the nuclei. There should be only few situations in which it crosses over the background (Fig. 4b) i.e. situations of big

distances between epithelial nuclei or in case of crypt breaks; in case this is not true, a FP crypt is detected [1]. The FP boundaries are depicted with red in Fig. 4a and the true positive (TP) inner boundaries with green.

5 Experimental results

The evaluation of the proposed methods (based on the hierarchical respective pyramid representation) has been performed on the same image set. Since a database with ground truth segmentations for this type of images does not yet exist, a pathologist has been asked to validate the results. The segmentation quality is established by visual inspecting the number of the mis-segmented nuclei per crypt.

Table 1 presents the results of testing the segmentation method on two datasets of images from tissues of two patients; some images are shown in Fig. 1a, Fig. 4, Fig. 6. and Fig. 7. The results confirmed that the proposed method could efficiently segment the crypts with a high degree of accuracy.

From the first set (Table 1, first row), a number of 87 crypts have been analysed resulting in 284 over segmented nuclei. Considering an average of 55 nuclei per crypt, the over-segmented nuclei represent 5.93% from the total crypt's nuclei (an average accuracy of 94.07% per crypt).

The second set was chosen from a patient with in a more advanced stage of the disease leading to higher number of over-segmented nuclei due to reactions that appeared between the crypts and the stroma.

Patient	Crypts	Average nuclei per crypt	Number of over-segmented nuclei	Over-segmented percentage per crypt	Average accuracy
1	87	55	284	5.93%	94.07%
2	71	55	312	7.98%	92.02%

Table 1 Segmentation evaluation results over two image sets from two patients.

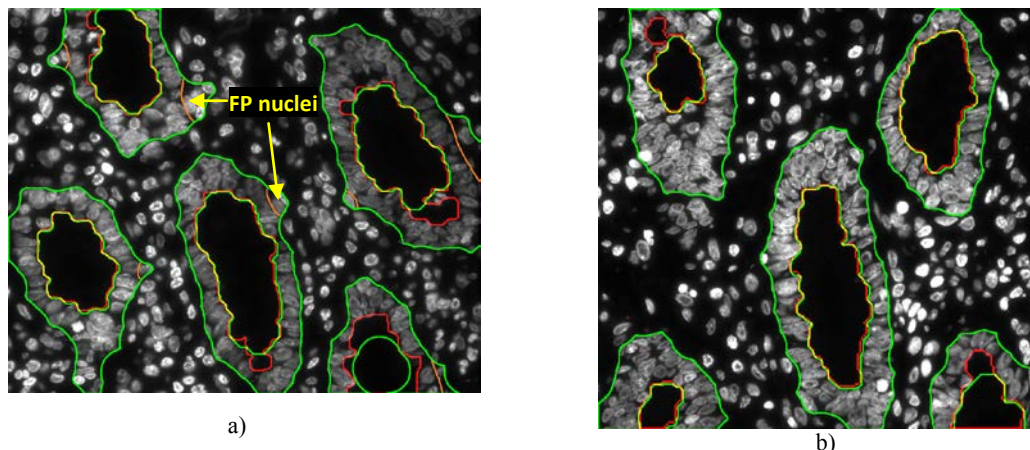


Fig. 6. The interior boundaries obtained using the morphological hierarchy (green curves) and the pyramid (red curves); the results are identical on the yellow portions. The outer borders are depicted with green.

5.1 Discussions and limitations

In this sub-section some limitations are highlighted and a more detailed study on the conditions that the objects of interest (i.e., lumen) must fulfil such that the technique provides satisfactory results. Also, some situations not suitable for the proposed technique are focused. In order to extend these methods on other images with human body cell nuclei from different tissues types but also in any other field in which the objects of interest have the features considered in designing these techniques, the restrictions and the limitations must be pointed out to the scientific community.

In Section 2.2, the criterion used to prevent the SE from growing too large was to limit the SE's size to cover a maximum number of 2-3 nuclei such that the gaps from the epithelial layer are filled. This condition is imposed by considering the biological structure of the crypts and proved to offer good results. This was also formulated in terms of *r-regularity*, (section 2.1). If the input objects to be detected do not respected this condition the method will not provide satisfactory results. For instance, the left lumen from Fig. 7a contains an unexpected big gap in the epithelial layer which was not filled by the closing operation. As a result, the lumen was merged with the stroma giving a false negative result (Fig. 7b).

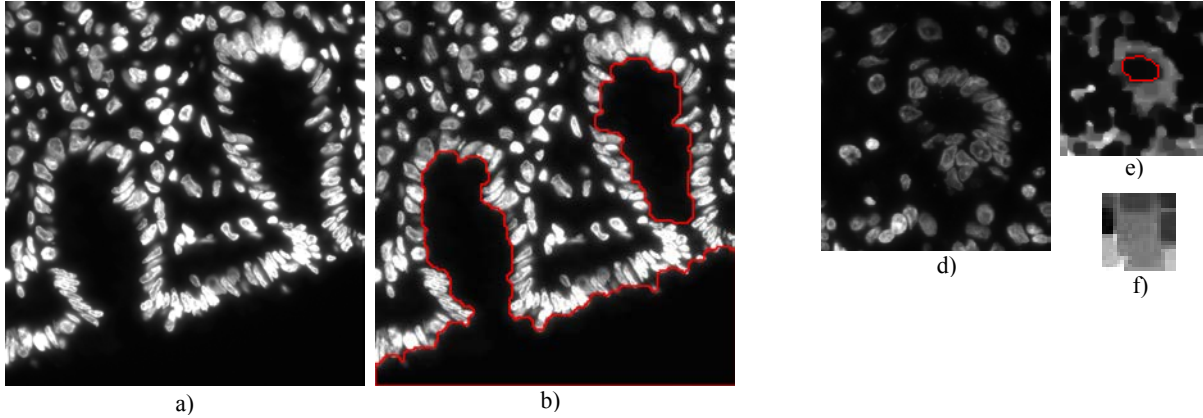


Fig. 7. Two situations in which the proposed techniques fail due to unexpected big gap in the epithelial layer (a, b) and a smaller lumen d). In d) a smaller lumen is shown; even that in the third level e) the lumen could be easily segmented, on the critical level f) this has been filled together with the gaps. The images e) and f) have been enlarged for better visualization.

The method also fails in situations of very elongate lumens. E.g. if the lumen is approximated with an ellipse, wrong results appear for ellipses with high eccentricity even that there is no break in the epithelial layer. The fail reason is related to the SE's size used to close the image. The epithelial will be merged in the areas where the lumen's diameter is close to the maximal SE's size.

Instead of making assumption on the lumen elongation, we ensure that the method provides satisfactory results if the minimum diameter of the lumen (inside distance between crypts walls) is big enough in comparison to the chosen SE's size. This is translated to a rule using the distance transform (DT) [18] by considering the epithelial layer as the nonzero regions. The DT will assign big values for the pixels near the lumen center. The possible failed situations can be identified by relating the maximum d_t of the DT values for the pixels inside the lumen with the used SE $\psi : \delta(d_t, \psi)$. δ must ensure that the SE does not fill the lumen on the upper levels and should impose for a crypt a SE with a radius r smaller than the maximum d_t

$$\alpha r < d_t, \alpha > 1 \quad (6)$$

where α is a weighed factor. This situation is exemplified using the lumen from Fig. 7d. Even that in the third level of the pyramid (Fig. 7e) the lumen can be segmented, on the 5th level (critical level Fig. 7f) this was merged with the gaps and the epithelial layer by the big SE.

The discussion from section 3.3 regarding the limitation of the RF proves its straightness and importance in this situation. Using the eq. (1 (section 3.1)), for each object, depending on its size, the proper critical level can be estimated such that the corresponding region from the base properly approximates the object. Since the lumen's size from Fig. 7d is smaller, a lower level should be selected; this level is obtained by using the eq. 5.

6 Conclusions

This work provides a detailed analysis of the hierarchical structures used in microscopic image segmentation. A comparison between the structures without, respectively with the sampling step is presented in order to highlight the advantages of the pyramid. Due to the properties needed to fill the gaps in the epithelial layer, the morphological closing filter was used to create these structures.

The lumen detection based on the morphological hierarchical structure provides good results but we proved that its used memory and computation time can be drastically reduced. By making use of the morphological pyramid, the used memory decreased from $25 \cdot \text{size}(I) = 22.5 \text{ MB}$ to $4/3 \cdot \text{size}(I) = 1.2 \text{ MB}$ where $\text{size}(I) = 0.9 \text{ MB}$. The computation time for each level (related to the number of processed pixels) decreases exponentially as going to the top levels in the pyramid's case, while for the hierarchy it increases based on a quadratic polynomial. The logarithmic height of the pyramid, instead of a linear one for the hierarchy, makes the top-bottom crossing faster.

In order to extend this coarser-to-fine approach on images with human body cell nuclei from different tissues types (e.g. prostate, breast or lung) but also in any other field in which the objects of interest have the features considered in designing this method, a set of restrictions and limitations have been rigorously formulated.

The SE used in the filtering operation was formulated in terms of *r-regularity* (section 2.1) and related to the biological information, i.e. the gap size. The formula used to compute the RF for a pixel from any level of the pyramid is used to determine the minimum levels of the pyramid to be computed in order to reduce the computation time and the used memory (section 3.1). In section 3.3 the limitation of the objects to be detected is formulated in terms of the RF's size in order to estimate the success application of the method on different image types.

This study will be continued by analysing the topological properties of the graph associated to the tissues components. Considerable effort will be spent to obtain a database with ground-truth segmentations and to find rigorous evaluation criteria of the results.

Acknowledgments. This work was supported in part by the "BRAIN - An Investment in Intelligence" doctoral Scholarship Program within the Technical University of Iasi, Romania and by the Austrian Science Fund under grant no. P20134-N13.

References

1. Smochina, C., Manta, V., Kropatsch, W.G.,” Semantic segmentation of microscopic images using a morphological hierarchy. 14th International Conference on Computer Analysis of Images and Patterns, pp. 102--109 (2011).
2. Ta, V.T., Lezoray, O., El Moataz, A., Schupp, S.: Graph-based tools for microscopic cellular image segmentation. *Pattern Recognition*, vol. 42(6), pp. 1113--1125 (2009).
3. Nattkemper, T.W.: Automatic segmentation of digital micrographs: A survey. *Journal Studies in health technology and informatics*, vol. 107(2), pp. 847--852 (2005).
4. Wu, H.S., Xu, R., Harpaz, N., Burstein, D., Gil, J.: Segmentation of intestinal gland images with iterative region growing. *Journal of Microscopy*, vol. 220(3), pp. 190--204 (2005).
5. Farjam, R., Soltanian-Zadeh, H., Jafari-Khouzani, K., Zoroofi, R.A.: An image analysis approach for automatic malignancy determination of prostate pathological images. *Clinical Cytometry*, vol. 72B (4), pp. 227--240 (2007).
6. Gunduz-Demir, C., Kandemir, M., Tosun, A.B., Sokmensuer, C.: Automatic segmentation of colon glands using object-graphs. *Medical Image Analysis*, vol. 14(1), pp. 1--12 (2010).
7. Naik, S., Doyle, S., Feldman, M., Tomaszewski, J., Madabhushi, A.: Gland segmentation and computerized Gleason grading of prostate histology by integrating low-, high-level and domain specific information. In: 2nd MICCAI Workshop Microscopic Image Analysis with Appl. in Biology, Piscataway, NJ, USA, (2007).
8. Humphries, A., Wright, N.A.: Colonic Crypt Organization and Tumorigenesis: Human Colonic Crypts. *Nature Reviews Cancer*, vol. 8(6), pp. 415--424 (2008).
9. Morikawa, K., Yanagida, J.: Visualization of individual DNA molecules in solution by light microscopy: DAPI staining method. *Japanese Biochemical Society*, vol. 89(2), pp. 693--696, Tokyo (1981).
10. Kropatsch, W.G., Haxhimusa, Y., Ion, A.: Multiresolution Image Segmentations in Graph Pyramids. In Kandel, A., Bunke, H., Last, M. editors, *Applied Graph Theory in Computer Vision and Pattern Recognition*. Springer Wien New York, vol. 52, pp. 3--41 (2007).
11. Gonzalez, R.C., Woods, R.E.: *Digital Image Processing* (third edition), Reading, Massachusetts: Addison-Wesley (1992).
12. Haralick, R.M., Zhuang, X., Lin, C., Lee, J. S. J.: The digital morphological sampling theorem. *IEEE Trans. Acoust., Speech, Signal Processing*, vol. 37, pp. 2067--2090 (1989).
13. Otsu, N.: A Threshold Selection Method from Gray-Level Histograms. In: *IEEE Transactions on Systems, Man, and Cybernetics*. vol. 9(1), pp. 62--66 (1979).
14. Chen, C.H., Lee, G.G.: Image Segmentation Using Multiresolution Wavelet Analysis and Expectation-Maximization (EM) Algorithm for Digital Mammography. *International Journal of Imaging Systems and Technology*, vol. 8(5), pp. 491--504 (1997).
15. Roshni, V.S., Raju, G.: Image Segmentation using Multiresolution Texture Gradient and Watershed Algorithm. *International Journal of Computer Applications*, vol. 22(5), pp. 21--28 (2011).
16. Tolba, M.F., Mostafa, M.G., Gharib, T.F., Salem, M.A.: MR-Brain Image Segmentation Using Gaussian Multiresolution Analysis and the EM Algorithm. *Proc. ICEIS* (2), pp.165--170 (2003).
17. Smochina, C., Manta, V., Kropatsch, W.G.: Sampling step importance in hierarchical semantic segmentation of microscopic images. In *Proc. 15th International Conference on System Theory and Control*, pp. 570 (2011).
18. Breu, H., Gil, J., Kirkpatrick, D., Werman, M.: Linear Time Euclidean Distance Transform Algorithms, *IEEE Transactions on Pattern Analysis and Machine Intelligence*, vol. 17(5), pp. 529--533 (1995).
19. Meine, H., Köthe, U., Stelldinger, P.: A topological sampling theorem for robust boundary reconstruction and image segmentation. *Discrete Applied Mathematics*, vol. 157(3), pp. 524--541 (2009).
20. W. G. Kropatsch, Y. Haxhimusa, Z. Pizlo, and G. Langs. Vision pyramids that do not grow too high. *Pattern Recognition Letters*, 26(3):319--337, 2005.